Analyzing Post-fire Vegetation Dynamics with Ultra-high Resolution Remote Sensing Data

Oleg Petrov [1,2], Andrey Medvedev [2]

[1] Faculty of Geography and Geoinformation Technology, Higher School of Economics, Moscow, Russia – ogpetrov@edu.hse.ru
[2] Institute of Geography, Russian Academy of Sciences, Moscow, Russia – medvedev@igras.ru

Keywords: UAV, digital aerial photogrammetry, DSM and dense point cloud analysis, post-fire vegetation recovering, forest fires, tree segmentation

Abstract

Monitoring post-fire vegetation dynamics is essential for understanding forest recovery processes and informing management strategies. UAV-based ultra-high resolution multi-temporal imagery, combined with the Structure-from-Motion and Multi-View Stereo (SfM-MVS) workflow, provides a cost-effective and scalable solution for forest monitoring. However, challenges remain in co-aligning multi-temporal datasets, segmenting individual trees in dense canopies, and ensuring classification accuracy. This study presents a comprehensive workflow for post-fire forest monitoring using UAV imagery, covering data acquisition, co-alignment, tree segmentation, species classification, and biophysical parameter estimation using growth models. The workflow was tested on three sites in Central Yakutia, with varying post-fire regeneration scenarios. Co-alignment was applied to multi-temporal UAV datasets, and tree segmentation was performed using the algorithms developed for Airborne Laser Scanning (ASL) forest point clouds. Tree species classification relied on statistical spatial variables of point clouds, and growth models were used to estimate parameters such as tree height, age, canopy area, above-ground biomass, and net primary productivity. The results demonstrated that co-alignment enabled consistent multi-temporal analysis, but performance was sensitive to flight planning consistency and lighting conditions. Tree segmentation accuracy was high in open-canopy areas but decreased in dense canopies. The classification of larch and birch species achieved relatively high precision and recall values, while dead trees showed lower classification accuracy due to challenging lighting conditions. Growth models successfully estimated biophysical parameters, but further validation using dendrochronological methods is required. This study highlights the potential of UAV-based multi-temporal monitoring for post-fire forest assessment. Future research should focus on improving tree segmentation of SfM-MVS point clouds in dense canopies, optimizing co-alignment under varying environmental conditions, and integrating additional point cloud classification methods to improve accuracy in areas with complex species distribution.

1. Introduction

Forest fires can have significant impacts on ecosystems, providing benefits such as encouraging reforestation (Lytkina, 2010), as well as drawbacks such as environmental damage and contributing to climate change (Narita et al., 2021). The implementation of an effective forest fire monitoring system, which integrates immediate fire detection with the analysis of associated impacts, is critical for mitigating these negative consequences (Chu and Guo, 2014). In this regard, remote sensing has become a superior approach for tracking forest fires and assessing their impact, offering advantages over conventional field-based methods in terms of efficiency and geographic coverage (White et al., 2016).

Traditional methods of forestation monitoring, which rely on the use of sample plots, have limitations in terms of accuracy and subjectivity of measurements and interpretation. These methods also involve significant costs associated with field monitoring. By contrast, remote sensing techniques can reduce the overall cost of research, particularly when applied to large study areas (White et al., 2016). There are a variety of remote sensing approaches that can be used for monitoring forestation, such as space- and airborne imaging from different sensor types, including optical, radar, and laser scanners. However, the data generated by these methods can vary significantly in terms of spatial and temporal coverage, resolution, spectral information, as well as other characteristics and challenges that should be taken into account when selecting a remote sensing approach (Chu and Guo, 2014).

Most of the publicly available data related to the goals of reforestation monitoring (Potapov et al., 2022; Lesiv et al., 2022; Potapov et al., 2021; Karra et al., 2021; Long et al., 2019; Krylov et al., 2014; Hansen et al., 2013; Sexton et al., 2013) are the result of analyzing satellite image mosaics with global coverage, obtained from various medium- and low-spatial-resolution imaging systems, such as Landsat (NASA, United States) and Sentinel (European Space Agency, European Union). In some cases, these data are supplemented with information from specific systems, as is the case with the Global Forest Canopy Height dataset, which relies on data from the Global Ecosystem Dynamics Investigation (GEDI) laser scanner, located on the International Space Station. For these datasets, most of the data is based on optical systems, using medium- and low-resolution multispectral imaging, which provides both acceptable spectral and spatial resolution, while also providing global coverage. It should be noted that the processing of such data requires significant computational power, due to the large volume of the data involved (Kutchartt et al., 2022). As a result, the datasets often have a temporal resolution ranging from one year to several years. Furthermore, datasets from recent years often utilize advanced satellite image processing techniques, such as convolutional neural networks and other machine learning algorithms (Piragnolo et al., 2021).

Remote sensing techniques are also used to collect large-scale data on the state of forest coverage and, consequently, for local monitoring of reforestation efforts (Pirotti et al., 2023). Two of the most widely used methods in this field are imaging from laser scanners mounted on UAVs and imaging from optical sensors also mounted on UAVs using photogrammetry techniques such as SfM (Cao et al., 2019; Wallace et al., 2016).

The two survey methods exhibit a high degree of similarity in the data they generate, as they both produce point clouds that reflect the three-dimensional structure of forests at a high level of spatial accuracy. However, there are also some differences between

them. Photogrammetric optical systems, for example, are unable to capture information through dense stands, and therefore cannot obtain data on the vertical distribution of vegetation in such circumstances. This is in contrast to methods that utilize laser scanners for generating point clouds (Wallace et al., 2016). At the same time, however, photogrammetric techniques in open stands achieve comparable accuracy to laser scans, while also being significantly less expensive (Cao et al., 2016). The low cost of implementation ultimately increases the spatial coverage of forest surveys due to the scalable nature of UAV surveys, which allows for more comprehensive data collection on forest cover.

Growth models provide essential information on the dynamics of key forest inventory indicators and form a crucial component of an efficient forest accounting and management system (Shvidenko et al., 2008). By utilizing growth models and site productivity data for a given forest area, it is possible to compute growth projections for individual tree species according to the specific regional forest conditions. For instance, tree height data can be used to estimate age and other forest inventory parameters, such as mean diameter, basal area, volume, and overall productivity. The modelling of these forest inventory indicators is based on the Von Bertalanffy Growth Function (VBGF), known in forestry literature as the Chapman-Richards function, which expresses inventory parameters as a function of age within a specific site productivity class (also known as bonitaet or site index) (Shvidenko et al., 2008). In addition to modelling key forest inventory indicators, ecological models have been developed to assess the ecological functions of forests, particularly biological productivity. The primary concept in this modelling framework is phytomass, expressed through two key metrics: net primary production (NPP), which represents the organic matter accumulated in plant tissues, calculated as the difference between gross production (total photosynthesis) and autotrophic respiration; and net ecosystem production (NEP), which is the difference between NPP and heterotrophic respiration of the forest ecosystem. These biological productivity models were also verified and validated (Shvidenko et al., 2008). As a result, growth modelling provides a broad range of applications, including estimating forest inventory parameters from limited data, such as remote sensing, and modelling ecological indicators, which is particularly significant in the context of global climate change.

Forest fires in central Yakutia cause a wide range of environmental and socioeconomic problems. However, there is also a beneficial impact associated with the fire-causing factor, which is one of the major factors in the forests of central Yakutia. This beneficial impact has been proven by A. I. Utkin and A. S. Isaev as cited in (Bartalev et al., 2015), and it is determined by the development of forests from regeneration to decomposition. Based on the early research conducted by forestry researchers in Central Yakutia on the impact of forest fires on forests (Lytkina, 2010), it appears that the role of forest fire in forest ecosystems is beneficial for larch. After fires, the position of larch is strengthened and relatively good regrowth of the original forest vegetation is observed. Forest fires also lead to alterations in the morphology of forest soil after the fires, as well as a lowering of the permafrost by tens of centimetres. Additionally, forest fires within the area of recurring ice spread contribute to the activation of thermokarst processes, which can lead to subsidence and slope failures, potentially delaying reforestation efforts for decades and centuries (Lytkina, 2010). At the same time, in regions with permafrost, where it is difficult for specialized forest fire prevention services to control, it is virtually impossible to prevent forest fires, as under conditions of inadequate mineralization of organic material in the soil and insufficient decomposition of plant debris, a sufficient accumulation of flammable material in forests in permafrost areas occurs to cause forest fires during periods of dry weather throughout the year (Lytkina, 2010). It should be noted that forest fires tend to occur cyclically, which is related to fluctuations in climate conditions from year to year, and this is particularly evident in central regions of Yakutia that are arid from a climatic standpoint (Lytkina, 2010). Therefore, taking into consideration both the positive aspect of forest fires under specific physiographic conditions in the forests of Central Yakutia, which act as a stimulant for reforestation in dense stand canopies, and the negative aspect for ecological communities resulting from the activation of thermokarst processes, which delay the reforestation process for decades and centuries, there is an urgent need for more in-depth monitoring of the reforestation process following pyrogenic impacts, including periodic monitoring.

The objective of this work is to analyze forest characteristics within the context of post-pyrogenic forest restoration. The primary method employed was multi-temporal UAV-based imaging, utilizing co-alignment procedure (Feurer and Vinatier, 2018), Structure-from-Motion (SfM) and Multi-View Stereo (MVS) methods to generate multi-temporal point clouds of the forest. The co-alignment method, which involves the simultaneous processing of images from different years during the Structure-from-Motion step, helps reduce the relative error between point clouds from different years (Nota et al., 2021). These point clouds were segmented down to the level of individual trees. The point clouds corresponding to individual trees were then classified according to species composition for the subsequent application of growth models, which enabled the estimation of other forest characteristics, such as age, diameter at breast height (DBH), stock volume, aboveground biomass, and net primary production (NPP). The obtained data were aggregated into a regular grid and then compared across different years. The goal of this study is to contribute to research on forest monitoring at the individual tree level through the use of optical multi-temporal UAV imaging and the results derived from these datasets.

2. Methodology

2.1 Study area

The model monitoring sites were selected from three areas in Central Yakutia (Figure 1a). The first site, “Viluy,” located 50 km west of Yakutsk, features a mixed species composition, primarily consisting of pine and larch, with a small proportion of birch (Figure 1b). In the larch forests of the "Viluy" site, a clear division into various age classes is observed, with a predominance of young growth. In the pine forests of “Viluy,” signs of low-intensity ground fires are evident. The second site, “Suola,” situated on the right bank of the Lena River in the Megino-Kangalassky district of the Sakha Republic, contains an area of burned forest with dead larch, as well as birch and larch young growth, along with sections of intact mature larch forests — the original forest type of this area (Figure 1c). The third site, “Alas,” located 1.5 km north of “Suola,” is distinguished by the presence of recent burn areas from 2021 (Figure 1d). Thus, the selected sites represent different forest types typical of Central Yakutia and various scenarios of pyrogenic disturbance.

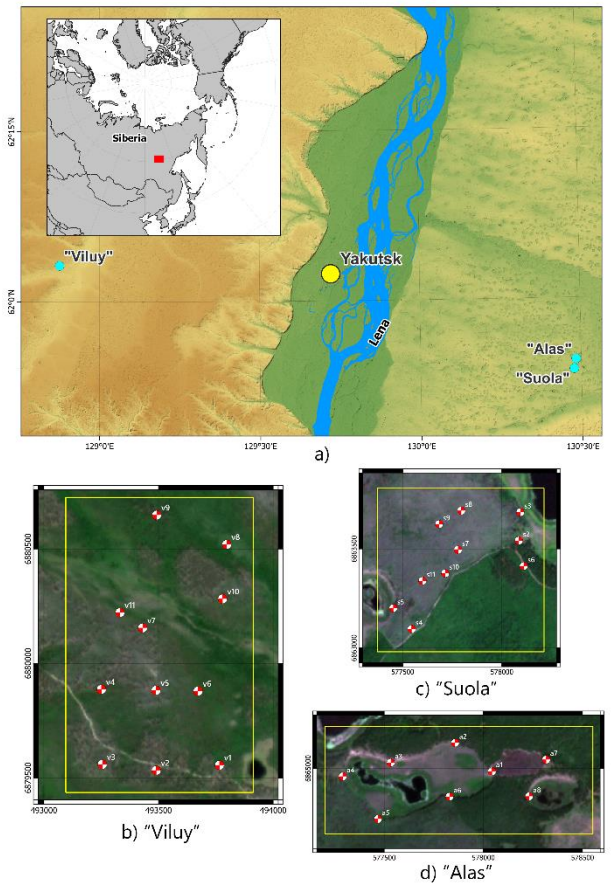

Figure 1. a) Study area; selected key sites with ground control points (GCPs): b) “Viluy” site, c) “Suola” site, d) “Alas” site. The coordinates of sites map are given in the CRS WGS84 UTM Zone 52N

2.2 Data acquisition

UAV surveys were conducted in 2019, 2021, and 2022. For the site “Viluy”, the imaging was performed in all of the listed years; for the site “Suola”, imaging took place in 2021 and 2022; and for the site “Alas”, imaging was conducted only in 2022. The UAV used for the imaging was a DJI Phantom 4 Pro V2.0. In 2019, the flight was conducted manually, while in 2021 and 2022, it was performed in automatic mode. Across all surveys, the flight altitude was consistently set to 100 m. Additionally, the 2021 imaging was conducted with a slight overlap between the image groups and under specific lighting, featuring long object shadows of the objects, to test the co-alignment method’s ability to link such groups during the Structure-from-Motion alignment phase.

To spatially reference the images, a network of ground control points (GCPs) was established to enhance the accuracy of spatial referencing (Figure 1b, 1c, 1d). The ground control points were set up prior to the 2022 imaging, so they only appeared in the images for one specific epoch. According to Nota et al. (2021), the presence of control points in just one dataset, processed through co-alignment, is sufficient to improve the absolute accuracy of spatial referencing. A total of 11, 10, and 8 control points were established for the “Viluy”, “Suola”, and “Alas” sites, respectively. The location data of the control points were collected using a Prince i30 PRIN. At the “Viluy” and “Alas” sites, a connection to the YKTS base station was established to obtain precise coordinates, while no such connection was available at the “Suola” site.

Additionally, four test plots were established, where data on the heights of individual trees and their diameters at breast height was collected using a laser rangefinder and manual measurements for validation purposes.

2.3 Data processing

The data processing was carried out using Agisoft Metashape Professional software (v. 1.7.1). The processing followed the sequence outlined below: 1) all images from different epochs were loaded into a single block during the alignment process, according to the co-alignment method (Feurer and Vinatier, 2018) and the image altitudes were adjusted using the relative altitude from metadata and the known absolute altitude of the flight start; 2) ground control points were included on all images they were fully visible, according to Nota et al. (2021); 3) the bundle adjustment step was performed (Optimize Cameras in Agisoft Metashape); 4) points of tie point cloud were filtered based on the parameters from Nota et al. (2021) using Gradual Selection in Agisoft Metashape — (i) present in less than three images, (ii) with a reconstruction uncertainty larger than 20, (iii) with a projection accuracy greater than 8, and (iv) a reprojection error larger than 0.5; 5) dense point clouds were generated. After the successful completion of the image alignment step (1–4), the tie point clouds were divided into separate blocks for the construction of dense point clouds (5). The following parameters were used during the image alignment step: Accuracy: High, Generic Preselection, Reference Preselection: Source, Key Point limit: 40,000 (default), Tie point limit: 4,000, Exclude stationary tie points, Adaptive camera model fitting. For the dense point cloud generation step, the following parameters were selected: Quality: High, Depth filtering: Mild, Calculate point colors.

During the processing of images for the “Suola” site, it was discovered that images from different years did not align when processed in a single block during the alignment step. To resolve this issue, the following method was proposed: 1) a set of images from a single year with GCPs (2022) was processed; 2) alignment was performed without bundle adjustment; 3) object coordinates were obtained from the aligned images for objects present in both years of imaging and unchanged in relation to nearby objects (fallen tree trunks, logs); 4) these objects were used as control points for the set of images which could not undergo co-alignment; 5) the alignment step was performed on this set of images using the obtained natural control points; 6) the alignment blocks were merged into a single block; 7) a bundle adjustment step was conducted on the merged block. Although this processing method does not fully replicate the co-alignment approach, the use of control points and the common bundle adjustment step still allows for a reduction in relative error.

2.4 Tree segmentation

The tree segmentation process was performed using the open-source R library *lidR* (Roussel et al., 2020), which implements most of the algorithms for processing airborne laser scanning (ALS) point clouds. Additionally, it supports point cloud processing by tiles, which reduces the hardware requirements. The process of generating individual point clouds for trees was divided into several steps. Initially, ground point clouds were classified using the Cloth Simulation Filtering (CSF) method (Zhang et al., 2016), with optimal parameters selected through experimentation: sloop_smooth = False, class_threshold = 0.2, rigidness = 3, as listed in *lidr* library. Subsequently, the point

clouds were normalised relative to the ground level using ground-class point cloud interpolation via the Inverse Distance Weighting (IDW) method. On the normalized point cloud, the tops of individual trees were identified using a local maximum filter. A dynamic window size was applied: a window size of 1 meter for points below 5 meters in height, a window size defined by the function $y = x \times 0.15 + 1$, for points between 5 and 20 meters (where x is the height of the point and y is the window size), and a window size of 4 meters for points above 20 meters. The normalized point clouds served as the foundation for constructing a canopy height model (CHM). The tree tops, in conjunction with the CHM, were employed to segment individual trees, employing the approach proposed in (Dalponte and Coomes, 2016).

2.5 Tree species classification

For each individual tree, the point cloud was classified into species using the CatBoost supervised machine learning algorithm (Prokhorenkova et al., 2019). The model's input parameters included spatial distribution characteristics of points within the cloud, as well as photogrammetric data on brightness. The parameters were calculated as follows: 1) vertical distribution parameter – the ratio of the standard deviation of the Z coordinate to the maximum value of the Z coordinate; 2) planar distribution parameter – the ratio of the standard deviation of the X and Y coordinates to the difference between the maximum and minimum values of the respective coordinates; 3) maximum height parameter – the maximum value of the Z coordinate; 4) canopy area parameter – the concave hull geometry area of points; 5) brightness indicator – the mean normalized value of the Red, Green, and Blue channels in the range from 0 to 1 (Dalponte et al., 2023).

The labels datasets for the model were collected during field research. Three main species were identified: larch, pine and birch, which differed in their spatial distribution of points, determining their shape and size. An additional category of standing deadwood was also included to enhance the model's precision. The data was randomly split into training, validation, and test sets with a 60/20/20 ratio. The training set was used independently for hyperparameter tuning using the Random Search method (Bergstra and Bengio, 2012: Gazzea et al., 2022). The validation set was used to evaluate the accuracy of the selected hyperparameters, while the combined training and validation sets were used for the final model training with the best hyperparameter values. The test set was used to calculate the final performance metrics of the classification model. Each model was trained on separate datasets, differing in surveying year and site, to compensate for variations in images acquisition.

2.6 Growth models

The species composition was then used in growth models (Shvidenko et al., 2008) to determine the age of the trees through the inverse growth function and tree height values. The growth (yield) models corresponding to the forest types of the studied area also require information on general bonitaet (site index), which was obtained during fieldwork. The obtained age values were used to calculate biophysical parameters using growth models and models of biological production: diameter at breast height (m), growing stock (m^3), above-ground biomass (t), and net primary production (NPP, $tC \cdot year^{-1}$).

3. Results

3.1 Validation using field data

In this section, the results of point cloud acquisition, individual tree segmentation, tree species classification based on point clouds, and the application of growth models for obtaining stand parameters will be considered.

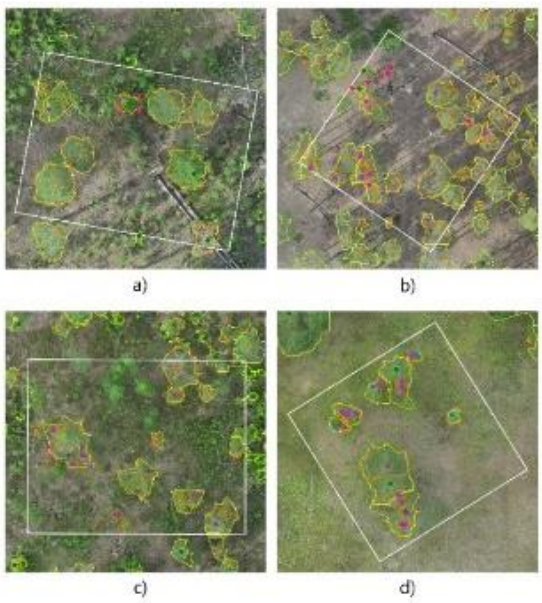

Figure 2. Validation plots. Green, orange, and blue points indicate the tree tops of pine, larch, and birch, respectively, as derived from segmented UAV point clouds. Pink points represent undetected tree tops. Yellow lines depict the concave hull geometry of the detected tree point clouds, while orange lines show the refined canopy boundaries based on field data.

The data obtained during fieldwork were employed to validate the measurement of tree height using SfM-MVS, tree segmentation approaches and tree species classification. General range of heights of detected trees was from 2.5 to 17.5 m, which is typical for larch and pine trees in study area. A comparison between the field data and the segmented tree point cloud from UAV imagery revealed that the root mean squared error (RMSE) of tree heights was slightly less than 1 m, and the mean absolute error (MAE) amounted to -0.016 m. It is worth noting that only half of the trees were identified based on the validation data due to the limited sample size used for validation purposes. Besides, some trees were mistakenly identified as existing trees, especially in the trees with wide crowns or a continuous canopy.

The species composition of the study area was verified using a field data label dataset on the test set, which was not used in hyperparameter tuning or model training. The larch and birch classes at the Suola site, where reforestation processes are ongoing and species boundaries are well-defined, exhibited high classification quality metrics (precision and recall: 0.85–0.9). In contrast, at the "Viluy" site, which has a dominant larch and pine composition with a mixed spatial distribution, lower classification quality values were observed. Additionally, the birch class at the "Viluy" site showed the lowest classification quality metrics due to its very low abundance in pine-larch forests.

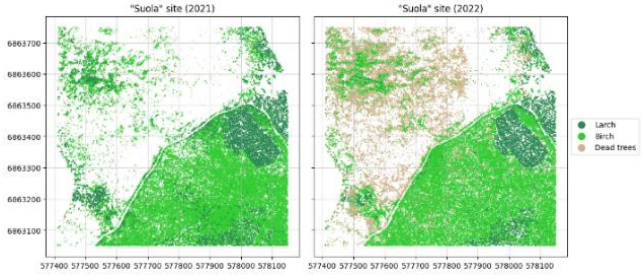

Figure 3. Tree species classification of segmented UAV tree point clouds. Size of the points depicts its normalized heights.

Dead trees (snags) also had low classification quality metrics, particularly in the 2021 datasets (Figure 3), likely due to challenging lighting conditions that resulted in long shadows, making snag identification more difficult. However, this class was used only as an auxiliary category and was not included in growth models applying. Given the high recall metrics for the main larch and birch classes, the low classification quality of this class can be considered negligible.

For each tree with height value and classified species all biophysical parameters were calculated: diameter at breast height, growing stock, above-ground biomass, and net primary production. The only biophysical parameter that could be compared was the diameter of tree trunk at the breast height, which was also collected during fieldwork. The analysis revealed a slight overestimation of the values of diameter by the model. The RMSEs, with a total spread of values ranging from 5 to 30 cm, were approximately 5 cm.

3.2 Maps of structural and biophysical parameters of forest

For each epoch and site, individual tree parameters calculated using growth models were aggregated into a regular grid for visualization purpose. These parameters are as follows: 1) Tree height defined as a maximum Z coordinate value of the points in the segmented tree point cloud; 2) Tree age estimated using a reverse growth model; 3) Tree cover calculated as the concave hull geometry area normalized by grid size; 4) Tree stock, 5) Tree above-ground biomass (AGB), 6) Tree Net Primary Productivity (NPP) – the last three parameters were estimated based on tree age value using growth models. Figure 4 present example of generated map with estimated parameters, illustrating clear spatial differentiation in the values of different tree species. Using the 2022 data for the “Suola” site as an example, the map illustrates a similarity between tree growth and age, as well as between timber stock and above-ground biomass (AGB). In contrast, net primary productivity (NPP) values differ from these patterns. Thus, the maps provide a clear representation of spatial differentiation and quantitative indicators of the structural and biophysical parameters of the forest stand.

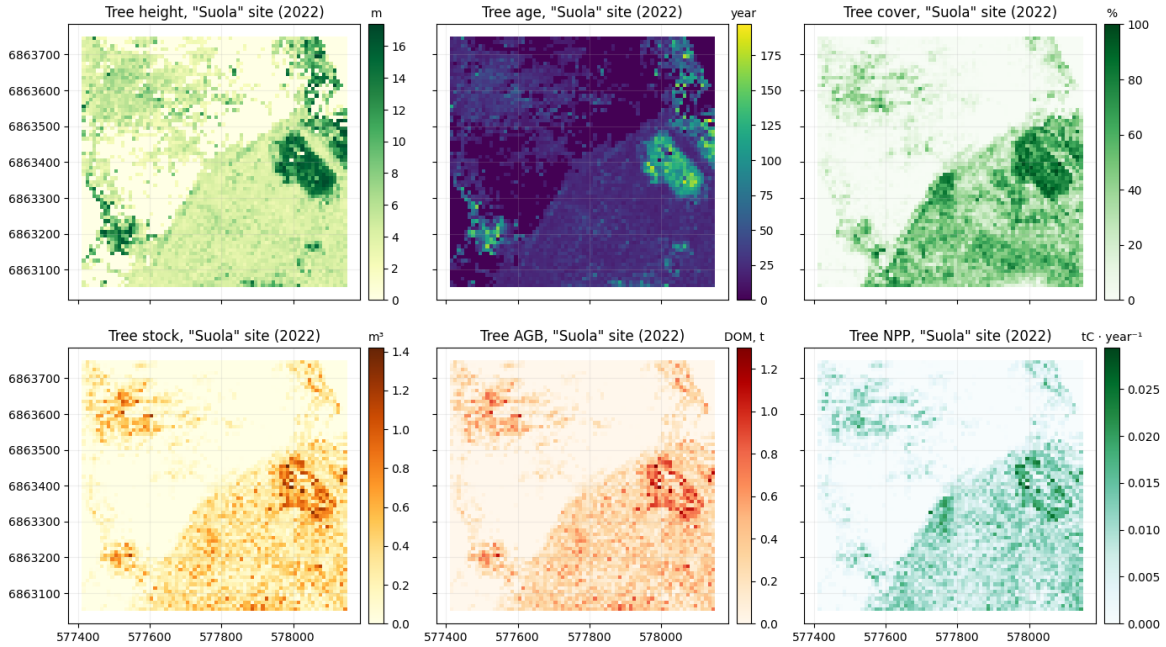

Figure 4. Individual tree structural and biophysical parameters aggregated on a 10 m regular grid at the “Suola” site (2022).

4. Discussion

The results of the full workflow for estimating tree parameters using multi-temporal UAV imagery lead to several assumptions and challenges.

In this study, we did not calculate relative errors between co-aligned multi-temporal datasets. However, based on the visual consistency of point clouds, these relative errors are assessed as acceptable. It was identified as crucial for UAV-SfM to maintain consistent survey planning, particularly ensuring similar image overlap across all datasets. In the “Suola” and “Viluy” UAV imagery datasets, insufficient overlap between image groups resulted in poor-quality outcomes. Additionally, similar lighting conditions are assumed to be an essential requirement for a successful co-alignment procedure. In cases where the co-alignment process is not feasible, our technique of linking images from different epochs using natural control points present in both datasets can be applied.

Tree segmentation algorithms, originally developed for processing airborne laser scanning (ALS) point clouds of forests (e.g., in Pirotti et al., 2017), have demonstrated high accuracy in areas with sufficient spacing between trees and open canopies, as observed through visual examination. However, in regions where canopies overlap or form a fully closed canopy, these algorithms may introduce significant errors. Addressing this limitation requires further research.

Tree species classification based on statistical variables of point cloud spatial distribution has shown relatively high accuracy for the main species classes. However, further research is needed to assess the significance of different variables and explore the potential use of more complex methods for point cloud classification.

The use of growth models demonstrated strong potential for estimating forest biophysical parameters. However, these estimates require validation using dendrochronological methods for tree age and bio-ecological methodologies for the remaining parameters. It is also important to note that the accuracy of growth model predictions in our workflow depends on the precision of tree height measurements obtained during tree segmentation and the accuracy of species classification.

5. Conclusion

This study presents a complete workflow for monitoring post-fire vegetation dynamics using UAV ultra-high-resolution multi-temporal imagery and the SfM technique. We identified challenges and areas for future research in the use of multi-temporal UAV imagery with the co-alignment approach. With improvements in key workflow steps, such as tree segmentation in closed-canopy areas, the proposed workflow has the potential to be applied for large-scale forest monitoring of post-fire vegetation processes.

Acknowledgements

The work was carried out with partial support from the state task FMWS-2024-0009 #1023032700199-9.

References

Bartalev S.A., Stytsenko F.V., Egorov V.A., Loupian E.A., 2015. Satellite-Based Assessment of Russian Forest Fire Mortality. *Lesovedenie*. 2, 83–94.

Burrell, A.L., Sun, Q., Baxter, R., Kukavskaya, E.A., Zhila, S., Shestakova, T., Rogers, B.M., Kaduk, J., Barrett, K., 2022. Climate change, fire return intervals and the growing risk of permanent forest loss in boreal Eurasia. *Science of The Total Environment*, 831, 154885.

Cao, L., Liu, H., Fu, X., Zhang, Z., Shen, X., Ruan, H., 2019. Comparison of UAV LiDAR and Digital Aerial Photogrammetry Point Clouds for Estimating Forest Structural Attributes in Subtropical Planted Forests. *Forests*, 10(2), 145.

Chu, T., Guo, X., 2014. Remote Sensing Techniques in Monitoring Post-Fire Effects and Patterns of Forest Recovery in Boreal Forest Regions: A Review. *Remote Sensing*, 6(1), 470-520.

Dalponte, M., Coomes, D.A., 2016. Tree-centric mapping of forest carbon density from airborne laser scanning and hyperspectral data. *Methods in Ecology and Evolution*, 7(10), 1236-1245.

Dalponte, M., ... Frizzera, L., Gianelle, D., 2023. Spectral separability of bark beetle infestation stages: A single-tree time-series analysis using Planet imagery. *Ecological Indicators* 153. https://doi.org/10.1016/j.ecolind.2023.110349

Gazzea, M., Kristensen, L.M., Pirotti, F., Ozguven, E.E., Arghandeh, R., 2022. Tree Species Classification Using High-Resolution Satellite Imagery and Weakly Supervised Learning. *IEEE Trans. Geosci. Remote Sensing* 60, 1–11. https://doi.org/10.1109/TGRS.2022.3210275

Hansen, M.C., Potapov, P.V., Moore, R., Hancher, M., Turubanova, S.A., Tyukavina, A., Thau, D., Stehman, S.V., Goetz, S.J., Loveland, T.R., Kommareddy, A., Egorov, A., Chini, L., Justice, C.O., Townshend, J.R.G., 2013. High-Resolution Global Maps of 21st-Century Forest Cover Change. *Science*, 342(6160), 850–853.

Karra, K., Kontgis, C., Statman-Weil, Z., Mazzariello, J.C., Mathis, M., Brumby, S.P., 2021. Global land use / land cover with Sentinel 2 and deep learning. *2021: IEEE International Geoscience and Remote Sensing Symposium IGARSS*, 4704–4707.

Krylov, A., McCarty, J.L., Potapov, P., Loboda, T., Tyukavina, A., Turubanova, S., Hansen, M.C., 2014. Remote sensing estimates of stand-replacement fires in Russia, 2002–2011. *Environmental Research Letters*, 9(10), 105007.

Kutchartt, E., Pedron, M., Pirotti, F., 2022. Assessment of Canopy and Ground Height Accuracy from Gedi Lidar Over Steep Mountain Areas. *ISPRS Annals of the Photogrammetry, Remote Sensing and Spatial Information Sciences* V-3–2022, 431–438. https://doi.org/10.5194/isprs-annals-V-3-2022-431-2022

Lesiv, M., Schepaschenko, D., Buchhorn, M., See, L., Dürauer, M., Georgieva, I., Jung, M., Hofhansl, F., Schulze, K., Bilous, A., Blyshchyk, V., Mukhortova, L., Brenes, C.L.M., Krivobokov, L., Ntie, S., Tsogt, K., Pietsch, S.A., Tikhonova, E., Kim, M., … Fritz, S., 2022. Global forest management data for 2015 at a 100 m resolution. *Scientific Data*, 9(1), 199.

Long, T., Zhang, Z., He, G., Jiao, W., Tang, C., Wu, B., Zhang, X., Wang, G., Yin, R., 2019. 30 m Resolution Global Annual Burned Area Mapping Based on Landsat Images and Google Earth Engine. *Remote Sensing*, 11(5), 489.

Lytkina, L., 2010: *Forest restoration on the burned areas of the Lena-Amga interfluve: Central Yakutia*. Nauka, Novosibirsk.
Narita, D., Gavrilyeva, T., Isaev, A., 2021. Impacts and management of forest fires in the Republic of Sakha, Russia: A local perspective for a global problem. *Polar Science*, 27, 100573.

Piragnolo, M., ... Grigolato, S., 2021. Responding to Large-Scale Forest Damage in an Alpine Environment with Remote Sensing, Machine Learning, and Web-GIS. Remote Sensing 13, 1541. https://doi.org/10.3390/rs13081541

Pirotti, F., Kobal, M., Roussel, J.R. 2017. A comparison of tree segmentation methods using very high density airborne laser scanner data. *The International Archives of the Photogrammetry, Remote Sensing and Spatial Information Sciences*, XLII-2-W7, 285–290. doi.org/10.5194/isprs-archives-XLII-2-W7-285-2017

Pirotti, F., Adedipe, O., Leblon, B., 2023. Sentinel-1 Response to Canopy Moisture in Mediterranean Forests before and after Fire Events. Remote Sensing 15, 823. https://doi.org/10.3390/rs15030823

Potapov, P., Hansen, M.C., Pickens, A., Hernandez-Serna, A., Tyukavina, A., Turubanova, S., Zalles, V., Li, X., Khan, A., Stolle, F., Harris, N., Song, X.-P., Baggett, A., Kommareddy, I., Kommareddy, A., 2022: The Global 2000-2020 Land Cover and Land Use Change Dataset Derived From the Landsat Archive: First Results. *Frontiers in Remote Sensing*, 3, 856903.

Potapov, P., Li, X., Hernandez-Serna, A., Tyukavina, A., Hansen, M.C., Kommareddy, A., Pickens, A., Turubanova, S., Tang, H., Silva, C.E., Armston, J., Dubayah, R., Blair, J.B., Hofton, M., 2021. Mapping global forest canopy height through integration of GEDI and Landsat data. *Remote Sensing of Environment*, 253, 112165.

Prokhorenkova, L., Gusev, G., Vorobev, A., Dorogush, A. V., Gulin, A., 2018. CatBoost: Unbiased boosting with categorical features. *Advances in Neural Information Processing Systems*, 31, 6639-6649.

Sexton, J.O., Song, X.-P., Feng, M., Noojipady, P., Anand, A., Huang, C., Kim, D.-H., Collins, K.M., Channan, S., DiMiceli, C., Townshend, J. R., 2013. Global, 30-m resolution continuous fields of tree cover: Landsat-based rescaling of MODIS vegetation continuous fields with lidar-based estimates of error. *International Journal of Digital Earth*, 6(5), 427–448.

Shvidenko, A.Z., Schepaschenko, D.G., Nilsson, S., Buluy, Y.I., 2008. Tables and Models of Growth and Productivity of Forests of Major Forest Forming Species of Northern Eurasia (Standard and Reference Materials). Federal Agency of Forest Management, Moscow, Russia.

Wallace, L., Lucieer, A., Malenovský, Z., Turner, D., & Vopěnka, P. 2016. Assessment of Forest Structure Using Two UAV Techniques: A Comparison of Airborne Laser Scanning and Structure from Motion (SfM) Point Clouds. *Forests*, 7(12), 62.

White, J.C., Coops, N.C., Wulder, M.A., Vastaranta, M., Hilker, T., Tompalski, P., 2016. Remote Sensing Technologies for Enhancing Forest Inventories: A Review. *Canadian Journal of Remote Sensing*, 42(5), 619–641.

Zhang, W., Qi, J., Wan, P., Wang, H., Xie, D., Wang, X., Yan, G., 2016. An Easy-to-Use Airborne LiDAR Data Filtering Method Based on Cloth Simulation. *Remote Sensing*, 8(6), 501.